# NUMERICAL AND EXPERIMENTAL INVESTIGATION OF INTERACTING PLUMES

**I.A. Chirokov[1], T.G. Elizarova[2], I. Gibek[3], J.-C. Lengrand [4]**

1. Moscow State University, Departement of Numerical Mathematics and Informatics, 119899 Moscow, Russia
2. Institute of Mathematical Modeling, Russian Academy of Science, 125047 Moscow, Russia
3. Centre National d'Etudes Spatiales, 18 av.Edouard Belin, 31401 Toulouse Cedex 4, France
4. Lab. d'Aérothermique du CNRS, 1C av. de la recherche Scientifique, 45071 Orléans Cedex, France. +33 2 38 25 77 19, fax +33 2 38 25 77 77, e-mail: lengrand@cnrs-orleans.fr

**Abstract:** The present work is an investigation of two plume interaction problems: the mutual interaction of two parallel plumes and the impingement of a plume onto a flat plate parallel to its axis. For both problems, the case of small and zero background pressure are considered. Computations were carried out based on quasigasdynamic (QGD) equations and compared with the experimental results obtained in the SR3 low-density facility of the Laboratoire d'Aérothermique. The computational problem under consideration is solved in a 3D formulation. The numerical algorithm is realized for a multiprocessor system with distributed memory. Numerical results are in reasonable agreement with the experimental ones and give access to some flow features not available from the experiment.

## 1. Context of the study

Scientific and technological space missions using micro or mini-satellites are generating growing levels of interest. Such missions complement large-scale programs and can respond more quickly to special science needs or new technologies. CNES has been developing new platforms for micro-satellites (satellites whose total launch mass is about 120 kg) and for mini-satellites (satellites whose total launch mass is about 500 kg). The platform for mini-satellites is called *PROTEUS* (Re-configurable Platform for Observation, TElecommunications and Scientific Uses). These platforms are designed to lower costs, so that it is possible to carry out a greater number of experiments. They will be valuable tools for space experimentation and for rapid demonstrations of the feasibility of new concepts. Their in-orbit lifetime will be about three years.

**Micro-satellite platform.** The micro-satellite product line project, called *MYRIADES*, started owing to a strong demand from the French science community. The platform is being designed for the broadest possible spectrum of applications, built whenever possible around standard subsystems to minimize development costs. The first selected missions are *DEMETER* (Detection of Electro-Magnetic Emissions Transmitted from Earthquake Regions) in 2003 and *PARASOL* in 2004.

**Mini-satellite platform.** The *PROTEUS* platform has been developed to meet the need for a greater flexibility and lower costs. It can easily be adapted from one mission to the following one, and can be offered to the international market as a competitive product. The first satellite, which will use this platform, is *JASON*. It has been developed in co-operation between CNES and NASA, in order to replace *TOPEX-POSEIDON* (ocean topography). It will be launched in December 2001. *PICASSO-CENA*(climate study) will be launched in 2003 and *COROT* (stellar observatory) in 2004.

**Plume effects.** The propulsion subsystems of the micro-satellite platform (whenever propulsion is required) and of the mini-satellite platform are hydrazine propulsion subsystems. In particular, they consist of four thrusters whose thrust is one Newton at the beginning of the mission. The thrusters are all located on the same side of the satellite. As the satellites are small (side of about 1 m×1 m for a mini-satellite, side of about 0.6 m×0.6 m for a micro-satellite), the thrusters are very close to one another, which is unusual. During the satellite maneuvers, they are always activated at the same time. As far as plume effects are concerned, there is not any surface in front of the thrusters plumes. But a question has been raised: is there any risk of thermal or dynamic load, caused by the interactions of the plumes, for the surface on which the thrusters are located ? Indeed, sensitive equipment may be laid on this surface. That is why a study has been necessary. It started as an experimental work carried out in the SR3 low-density facility of the Laboratoire d'Aérothermique du CNRS on reduced-scale models that simulate real satellite configurations. It continues as a theoretical and numerical work to improve the prediction tools capable of treating the plume impingement problem.

**Present work.** A simplified configuration has been considered in the present work, consisting in two (instead of four) parallel plumes (twin plumes). The problem of a single plume interacting with a flat plate parallel to its axis has been also considered. It is very similar to the previous one because the flat plate replaces the symmetry plane of the twin

plume configuration. For both problems, numerical results have been compared with available experimental results.

In the flow under consideration the pressure and density vary strongly from the nozzle exit section to the external parts of the plume. The cross section of the plume changes dramatically from 2 millimeters near the nozzle to several centimeters at the downstream limit of the computational domain. These features require the implementation of fine computational grids, as well as a large number of iterative steps for convergence. The problem is very time consuming. In order to minimize computational time, the numerical algorithm has been realized for a powerful multiprocessor computational system.

Computations were carried out based on the quasigasdynamic (QGD) equations. Preliminary computational results for single and twin plumes were discussed in [1].

## 2. Experimental setup and results

Nitrogen jets were issued from one or two parallel conical nozzle(s) that simulated satellite control thrusters. The twin plumes (type I) were issued from a 15-degrees half-angle conical nozzle with critical radius $r_c = 0.2\,mm$, stagnation conditions $T_0 = 900\,K$ and $p_0 = 12$ bar. The single plume (type X) was issued from a 7-degrees half-angle conical nozzle with the same critical radius, stagnation conditions $T_0 = 1100\,K$ and $p_0 = 16$ bar. The distance between parallel axes of jets I was 50 mm and the distance between the axis of jet X and the flat plate, parallel to it, was 17 mm. Experimental investigations consisted in determining flowfield density by means of electron beam surveys and measurements of wall pressure and heat transfer rate.

Table 1 shows flow conditions and gas parameters corresponding to the experimental results, taken as conditions for the numerical simulation. Subscript $_e$ corresponds to the nozzle exit gas, $_\infty$ corresponds to the background gas, $_w$ corresponds to the gas at the wall. $Ma$ denotes the Mach number, $r_e$ the nozzle exit radius, $\lambda$ the mean free path, $Kn$ the Knudsen number ($Kn_e = \lambda_e/(2r_e)$), $\gamma = 1.4$ the specific heat ratio, $Pr = 14/19$ the Prandtl number. Experimental results for density distributions and wall pressure and heat transfer have been presented in [2]–[4].

| | Jet I | Jet X |
|---|---|---|
| $r_e$ (m) | $1.6 \cdot 10^{-3}$ | $1.7 \cdot 10^{-3}$ |
| $\lambda_e$ (m) | $1.304 \cdot 10^{-6}$ | $1.397 \cdot 10^{-6}$ |
| $Kn_e$ | $4.07 \cdot 10^{-4}$ | $4.1 \cdot 10^{-4}$ |
| $Ma_e$ | 5.781 | 5.813 |
| $T_e$ (K) | 117.1 | 141.8 |
| $p_e$ (Pa) | 954 | 1230 |
| $u_e$ (m/s) | 1275 | 1411 |
| $p_\infty$ (Pa) | 1 | 1 |
| $T_\infty = T_w$ (K) | 293 | 293 |

Table 1: Flow parameters

## 3. Quasigasdynamic equations

The numerical calculation is based on the quasigasdynamic (QGD) system of equations. The investigation of this system was done in, e.g. [7]. A review of theoretical and numerical results can be found in [8]. According to [7], the QGD equations can be interpreted as follows. Generally speaking gasdynamic system consists of three differential equations accounting for

conservation of mass (continuity equation)

$$\frac{\partial \rho}{\partial t} + \nabla_i J^i = 0, \tag{1}$$

conservation of momentum

$$\frac{\partial (\rho u^k)}{\partial t} + \nabla_i J^i u^k + \nabla^k p = \nabla_i \Pi^{ik}, \tag{2}$$

and conservation of total energy

$$\frac{\partial E}{\partial t} + \nabla_i \frac{J^i}{\rho}(E + p) + \nabla_i q^i = \nabla_i (\Pi^{ik} u^k). \tag{3}$$

To close the system (1)–(3), the mass flux vector $J^i$, the shear-stress tensor $\Pi^{ik}$, and the heat flux vector $q^i$ must be expressed as a function of macroscopic flow quantities, namely density $\rho$, velocity coordinates $u_i$, and pressure $p$. The particular Quasigasdynamic (QGD) system is obtained by taking

$$J^i = \rho(u^i - \frac{\tau}{\rho}\left(\nabla_j(\rho u^i u^j) + \nabla^i p\right)), \tag{4}$$

$$\Pi^{ik} = \Pi^{ik}_{NS} + \tau u^i \left(\rho u^j \nabla_j u^k + \nabla^k p\right) + \\ + \tau g^{ik} \left(u_j \nabla^j p + \gamma p \nabla_j u^j\right), \tag{5}$$

and

$$q^i = q^i_{NS} - \tau \rho u^i \left(u^j \nabla_j \varepsilon + p u_j \nabla^j (\frac{1}{\rho})\right). \tag{6}$$

Here $q^i_{NS}$ and $\Pi^{ik}_{NS}$ are the Navier-Stokes heat flux and shear-stress tensor, $g^{ik}$ is the metric tensor, $\mu$ and $\kappa$ are the viscosity and heat conductivity coefficients, $\eta$ is the second viscosity coefficient (bulk viscosity), $\varepsilon = p/(\rho(\gamma - 1))$.

For gases, the parameter $\tau$ is a relaxation time. For vanishing Knudsen numbers, it is defined as $\tau = \mu/p$ (Maxwell relaxation time).

For the QGD equations, mass, momentum, total energy, conservation laws and the entropy theorem

are valid as for the classic Navier-Stokes system. QGD and Navier-Stokes systems differ in the order of $O(\tau)$. For stationary flows the dissipative terms (terms in $\tau$) in the QGD equations have the asymptotic order of $O(\tau^2)$ for $\tau \to 0$, or in the dimensionless form of the equations, $O(Kn^2)$ for $Kn \to 0$. The boundary layer approximation for QGD equations leads to the classical Prandtl equation system. Examples of numerical simulation of the underexpanded jets based on QGD equations can be found in [9]–[12].

## 4. Problem formulation

The problem under consideration is solved in $(x, y, z)$ cartesian formulation [12]. The computational domain is shown in Fig. 1.

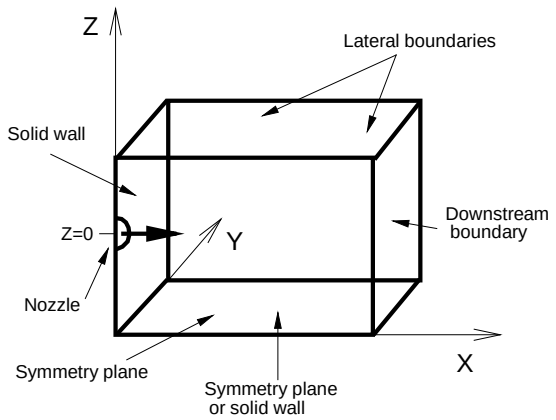


Figure 1: Computational domain

The QGD equations are supplemented with expressions for the total volumic energy $E = 0.5\rho(u_x^2+u_y^2+u_z^2) + p/(\gamma-1))$ and for the perfect gas equation of state $p = \rho\mathcal{R}T/\mathcal{M}$. The viscosity law is taken in the form $\mu \sim T^\omega$, $\omega$ is related to intermolecular interaction; for nitrogen $N_2$ we take $\omega = 0.75$. Here the parameter $\tau$ is taken constant and equal to: $\mu_e/p_e$.

As boundary conditions, slip conditions were used for the vertical solid wall (see 1) and for the plane (horizontal solid wall). Symmetry conditions were used to reduce the number of space grid nodes and "soft" conditions were used for the downstream boundary. The lateral conditions were different for the cases of zero and non-zero background pressure values. At the nozzle exit section the inflow profile was prescribed. It accounted for a laminar boundary layer profile [13].

## 5. Numerical algorithm and parallel realization

Numerical modeling of the jet flow is based on a finite-volume algorithm. The computational domain is covered with a rectangular non-uniform space grid. QGD equations are approximated by the finite-difference centered scheme, with space accuracy of $O(h^2)$. In order to stabilize the numerical solution an artificial dissipation of the order of $O(\beta h)$ is added to the terms that contain $\tau$. For the variants under consideration $\beta$ is equal to 0.5.

The finite-difference scheme was solved by an explicit algorithm where the steady-state solution is attained as the limit of a time-evolving process. The choice of the time step is based on the stability condition in the form

$$h_t = \alpha \min(h/c), \tag{7}$$

where $h$ represents the space grid step, and $c$ is the thermal velocity. Details of the computational algorithm can be found in [12].

The features of the flow require the implementation of fine computational grids, together with a large number of iterative steps for convergence. So the jet problem is time consuming and requires the implementation of powerful computer systems, namely parallel computers. The numerical method implemented here has internal structural parallelism and the use of parallel computers seems natural.

The Message Passing Interface (MPI) standard has been used for the organization of interprocessor data exchange. Calculations have been performed on cluster multiprocessor computer systems with distributed memory. Parallel code is constructed using a domain decomposition technique (the geometrical parallelism). This means that the whole computational domain is divided into subdomains in $x$-direction and each processor provides calculations in its own subdomain. The number of subdomains is equal to the number of processors used. In the present computational work, a cluster computer system consisting of 24 processors with distributed memory equipped with Intel Pentium III microprocessors was used. This system is located in the Lab. d'Aérothermique.

Efficiency estimations show that the implemented numerical algorithm (explicit in time and homogeneous in space approximation of QGD equations) allows an efficient use of cluster multiprocessor systems.

## 6. Computational results

Computations were carried out for flow conditions as close as possible to that of experiment (Table 1). Also calculations were made for slightly different configurations, not experimentally studied. The computational results are divided in four groups:

- A: twin parallel jets I with background pressure $p_\infty = 1$ Pa, distance between axes of jets $2H = 50$ mm, corresponding to experimental data;
- B: twin parallel jets I, same as A but with zero background pressure (no experimental results);
- C: single jet X with a parallel plate, background pressure $p_\infty = 1$ Pa, distance between axis of jet and plate $H = 17$ mm, corresponding to experimental data;
- D: twin converging jets I, angle between axes of jets is 26.5 degrees, zero background pressure, distance between axes of jets $2H = 50$ mm (same as B except convergence, no experimental results).

Dimensionless quantities were introduced based on nozzle exit gas parameters. However the computational results are presented in usual dimensional form. In the case of jets I (groups A, B and D) the computational grid ($N_x \times N_y \times N_z$) was $140 \times 43 \times 74$, the x-direction step $h_x = r_e = 1.6\,mm$, y- and z-directions minimal step $h_{yz} = r_e/2 = 0.8\,mm$.

For jet X (group C) the grid was $140 \times 42 \times 62$, the x-direction step $h_x = r_e = 1.7\,mm$, y- and z-directions minimal step $h_{yz} = r_e/2 = 0.85\,mm$.

In all cases $h_{yz}$ increased between adjacent cells by a constant factor 1.05 outside the jets (jet-plate) area.

The number of time steps to achieve stable solution is of the order of $10^4$–$10^5$, which takes about 10 hours machine time of 8 Pentium III processors, working in parallel.

### 6.1. Results for twin jets I, background pressure 1 Pa (group A)

Fig. 2 represents the calculated number density contours in the $(x, y = 0, z)$ plane. On the figures the computational domain was doubled according to the symmetry plane conditions. Number density was normalized by stagnation number density $n_0 = 9.657 \times 10^{25}$ m$^{-3}$. In the present numerical results, the interaction between the jets begins at a distance $x$ somewhat smaller than in the experiment. Except for this small difference, the calculated contours match well the experimental ones ([2], Fig. 3-4, [3], Fig. 18 or [4], Fig.29).

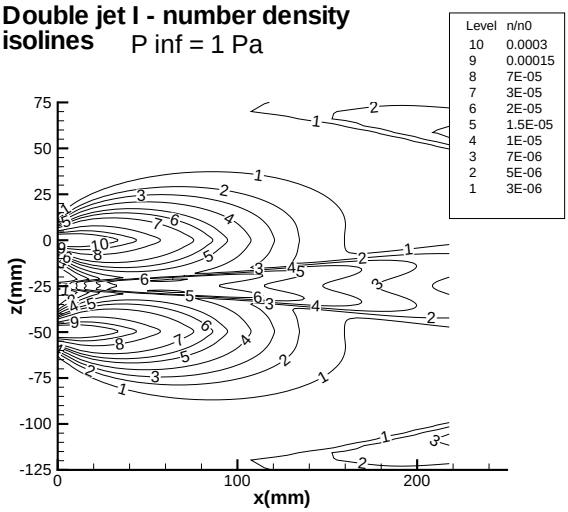


Figure 2: Calculated density contours

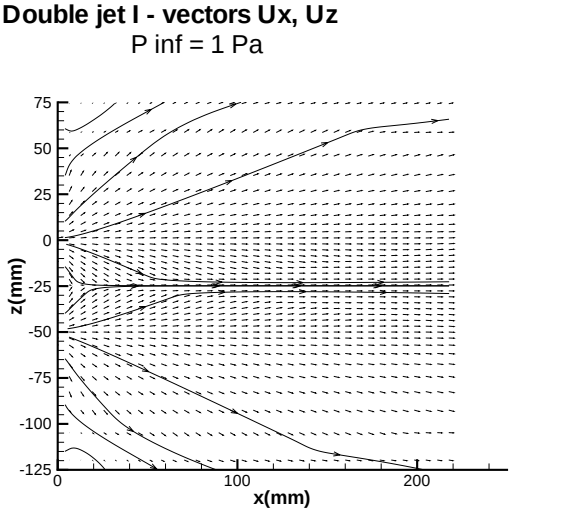


Figure 3: Calculated velocity vectors

Fig. 3 shows the calculated velocity vectors in the same plane and some streamlines. Note that there is no backward flow.

Fig. 4–5 represent on-axis values ($z = 0, y = 0$) for number density, normalized by the stagnation number density $n_0 = 9.657 \times 10^{25}\,\mathrm{m}^{-3}$, and for Mach number. They are compared with experimental results taken from [3], Table 3, or from [4], Table 3. $x$ is normalized by $r_c = 0.2$ mm. The density distribution is close to the experimental one. It is quite insensitive to the background pressure. The jet interaction is visible at large abscisses on numerical results, whereas it does not yet appear in the experimental results.

For the large abscisses the calculated values of the Mach number are smaller then those estimated from

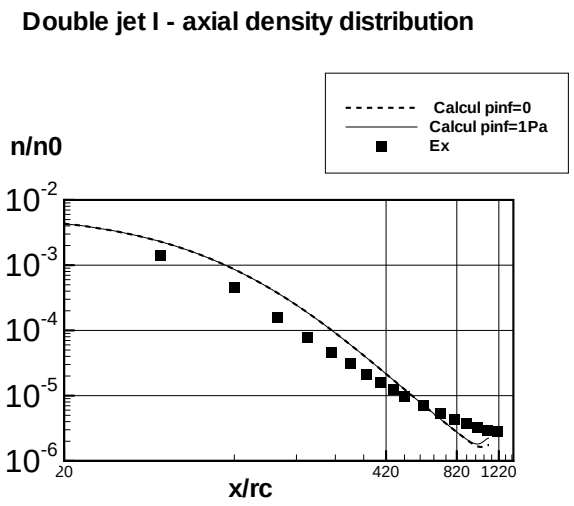


Figure 4: Axial density distribution

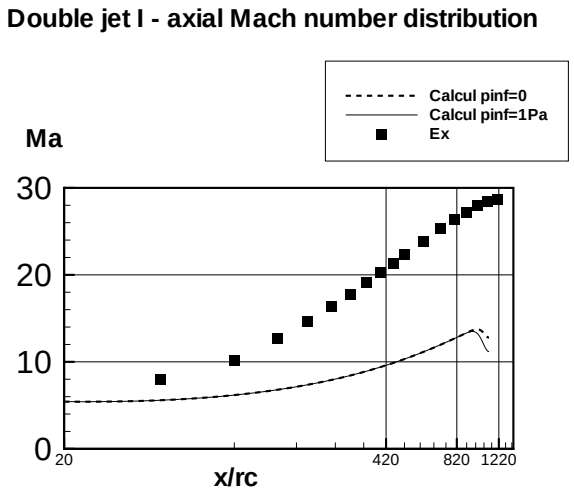


Figure 5: Axial Mach number distribution

the experiments using a Pitot tube. The discrepancy occurs in a domain where the gas temperature is only a few Kelvin and the Mach number values are not significant because of strong translational nonequilibrium, which affects the Pitot pressure measurements.

Fig. 6 presents transverse number density profiles. They are in good agreement with the experimental results ([3], Figs. 16 and 17, or [4], Fig. 25.)

### 6.2. Results for twin jets I, zero background pressure (group B)

Fig. 7, 8, 9 show calculated data, corresponding to that presented in Fig. 2, 3, 6, respectively, but for zero background pressure. They are very close to the group A results.

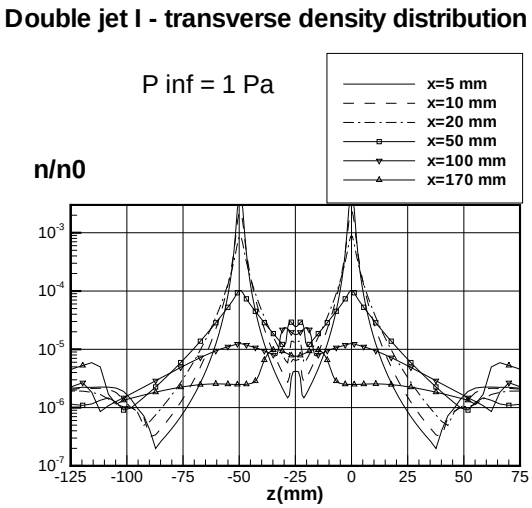


Figure 6: Calculated transverse density distribution

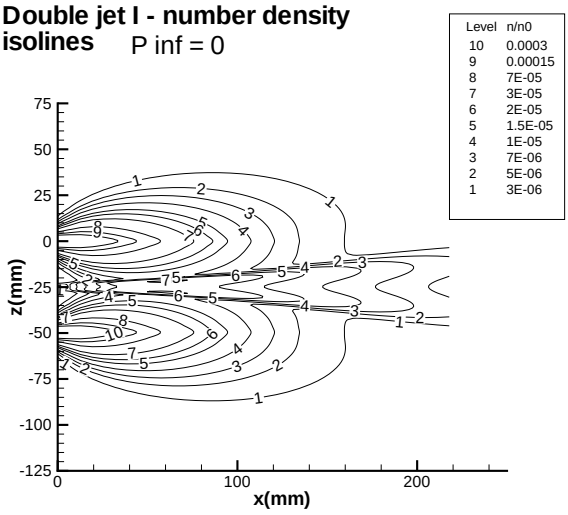


Figure 7: Calculated density contours

### 6.3. Results for single jet X with parallel plate (group C)

Fig. 10 represents the calculated number density contours in the $(x, y = 0, z)$ plane. Number density was normalized by stagnation number density $n_0 = 1.054 \times 10^{26}$ m$^{-3}$. The calculated contours match well the experimental ones ([4], Fig.24).

Fig. 11 shows the calculated velocity vectors in the same plane and some streamlines. Note that there is no backward flow also.

Fig. 12–13 depict transverse number density profiles. They are in good agreement with the experimental results (see [4], Fig. 21, 22.)

Fig. 14–15 represent longitudinal on-plate values $(z = -17\,mm, y = 0)$ of pressure and normal ther-

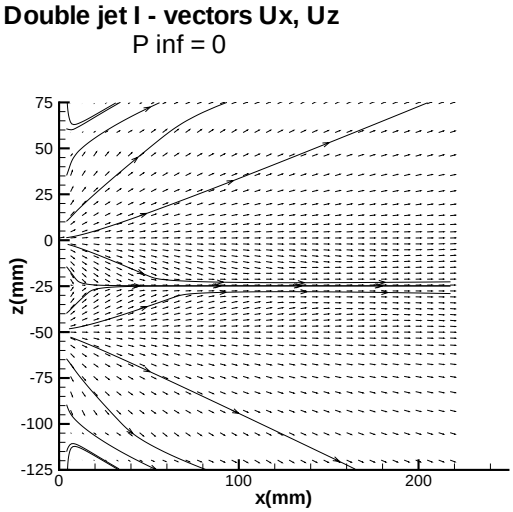


Figure 8: Calculated velocity vectors

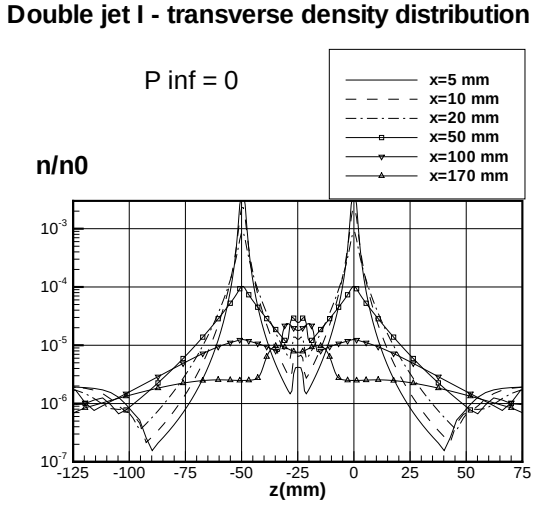


Figure 9: Calculated transverse density distribution

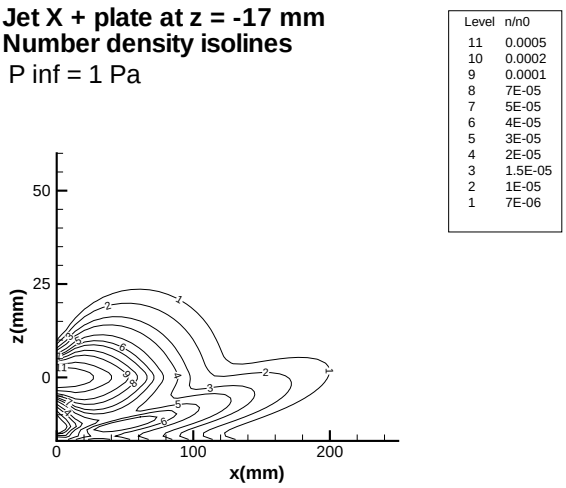


Figure 10: Calculated density contours

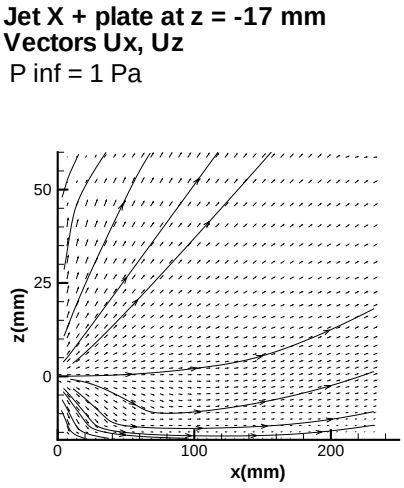


Figure 11: Calculated velocity vectors

mal flux. They are compared with experimental results, taken from [5], Fig. 5 and from [6], Table 2A.

Fig. 16 presents transverse on-plate ($x = 40$ mm, $z = -17$ mm) pressure distribution, also compared with experimental results, taken from [5], Fig 7.

### 6.4. Results for converging jets I (group D)

The conditions are the same as for group B, except the jets converge rather than being parallel.

Fig. 17 represents the calculated number density contours in the $(x, y = 0, z)$ plane. On the figures the computational domain was doubled according to the symmetry plane conditions. Number density was normalized by stagnation number density $n_0 = 9.657 \times 10^{25}$ m$^{-3}$. The resulting jet (between initial jets) is denser and thicker than that on Fig. 7.

Fig. 18 shows the calculated velocity vectors in the same plane and some streamlines. There is no backward flow, as for group B (Fig. 8).

Fig. 19 presents transverse number density profiles. The denser central jet (compared to that on Fig. 9) is clearly visible.

## 7. Conclusion

Numerical results exhibit a good global agreement with experiment, and provide information on those quantities not measured in the experiment, e.g. the absence of the recirculation zone between twin jets.

**Acknowledgement.**
This work was supported by the French Space Agency

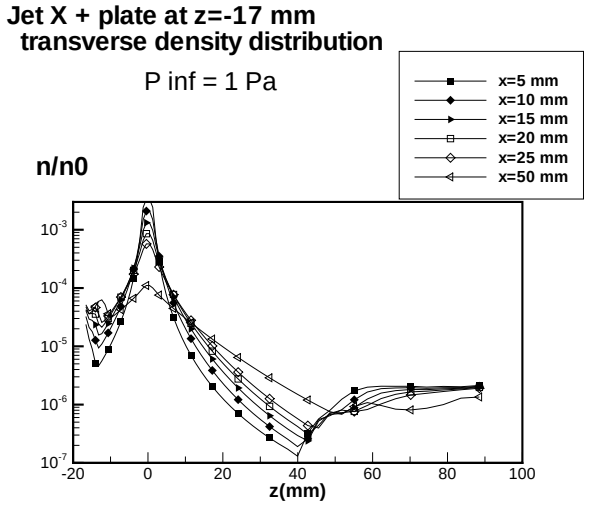


Figure 12: Calculated transverse density distribution, part 1

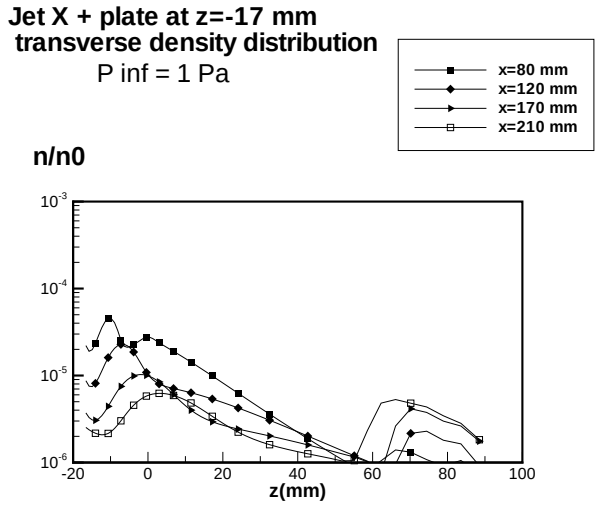


Figure 13: Calculated transverse density distribution, part 2

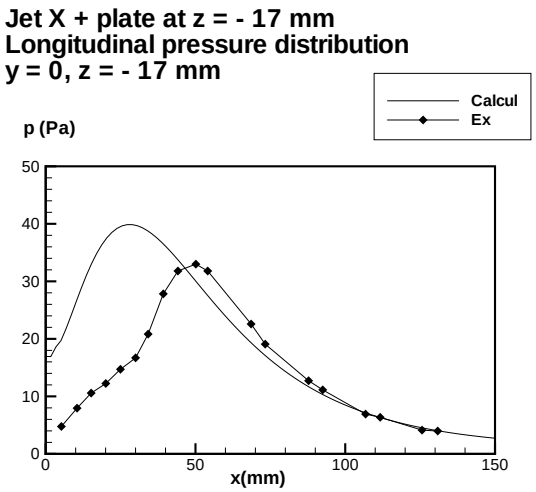


Figure 14: On-plate pressure distribution

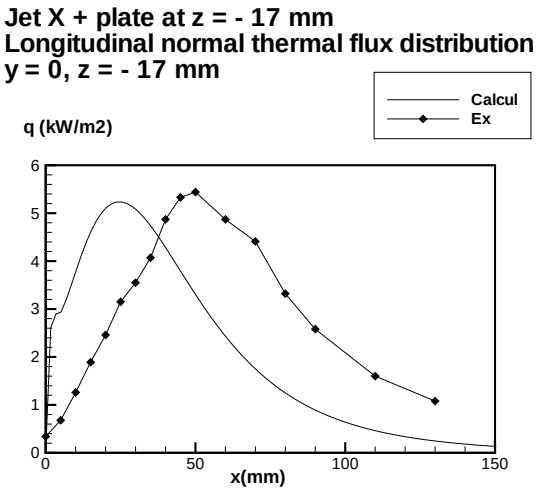


Figure 15: On-plate thermal flux distribution

CNES under contract 712/CNES/99/7633/01.

## References

[1] Allègre J., Chirokov I.A., Gorchakova N.G., Graur I.A., Purpura C., Gibek I., Elizarova T.G., Lengrand J.-C.: Numerical and experimental investigation of plumes interacting with satellite walls. Proc. 3rd Intern. Conf. on Spacecraft Propulsion, ESA SP-465, pp. 619–626, Dec.2000.

[2] Allègre J., Lombardo G., Lengrand J.-C.: Interaction entre deux jets et une paroi de satellite. Lab. d'Aérothermique du CNRS, RC 99-1, Janv.1999.

[3] Allègre J., Chaix A., Lengrand J.-C.: Etude expérimentale de la densité dans des jets sous-détendus. Lab. d'Aérothermique du CNRS, NT 99-1, Sep.1999.

[4] Allègre J., Chaix A., Gorchakova N.G., Purpura C., Lengrand J.-C.: Etude expérimentale de jets propulsifs issus de tuyères parallèles. Lab. d'Aérothermique du CNRS, NC 2000-1, Sep.2000.

[5] Allègre J., Bisch D., Lengrand J.-C.: Impact de jets sur des parois: Mesures de pression et visualisations. Lab. d'Aérothermique du CNRS, RC 96-1, Janv. 1996.

[6] Allègre J., Lengrand J.-C.: Impact de jets sur des parois: Mesures de flux thermique. Lab. d'Aérothermique du CNRS, RC 96-3, Oct. 1996.

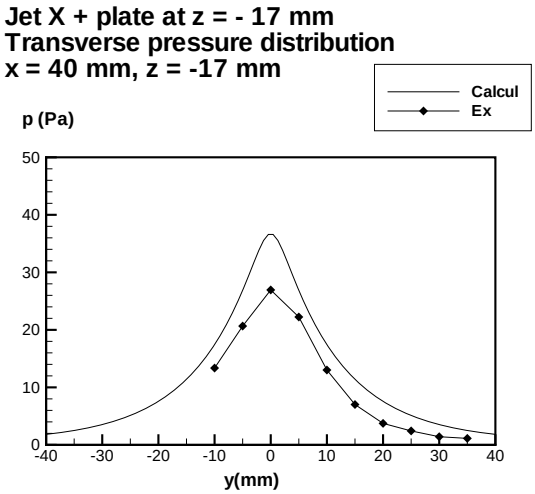


Figure 16: On-plate pressure distribution

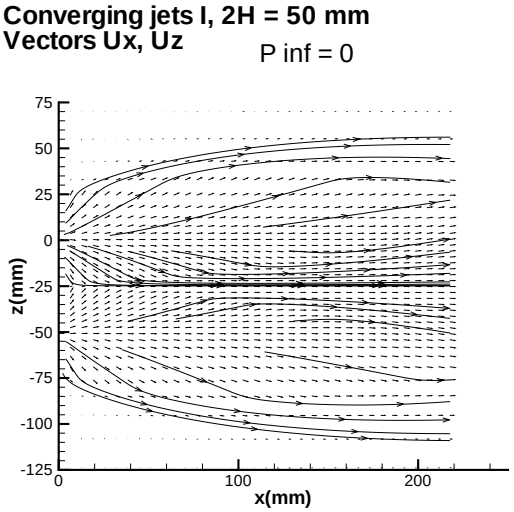


Figure 18: Calculated velocity vectors

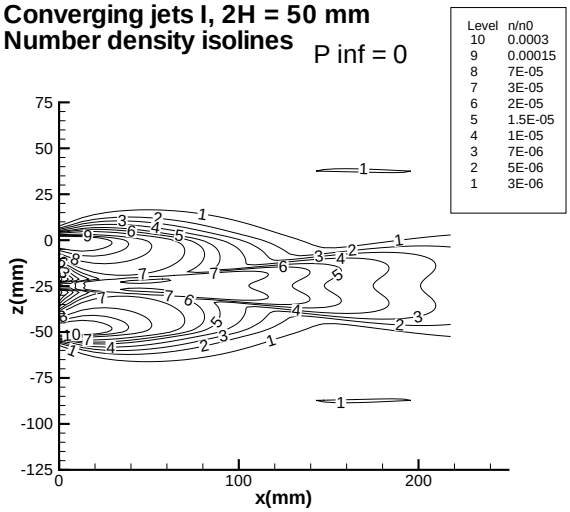


Figure 17: Calculated density contours

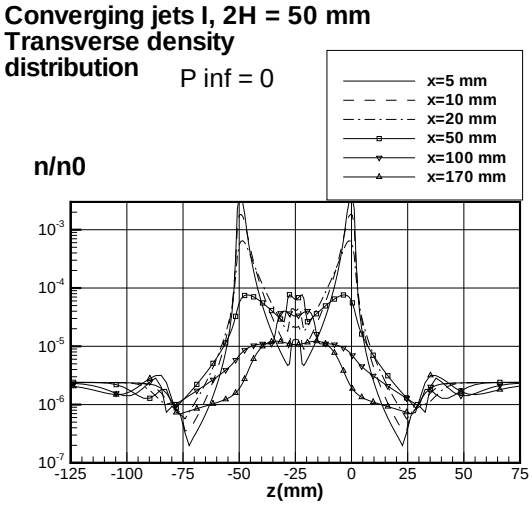


Figure 19: Calculated transverse density distribution

[7] Sheretov Yu.V.: Quasihydrodynamic equations as a model for viscous compressible heat conductive flows, in book: Implementation of functional analysis in the theory of approaches, Tver University, 1997, pp.127–155 (in Russian).

[8] Elizarova T.G., Sheretov Yu.V.: Theoretical and numerical investigation of quasigasdynamic and quasihydrodynamic equations. Comput. Mathem. and Mathem. Phys., 2001, V.41, No 2, pp. 219–234.

[9] Mate B., Graur I.A., Elizarova T.G., Chirokov I.A., Tejeda G., Fernandez J.M., Montero S.: Experimental and numerical investigation of an axisymmetric supersonic jet. Journal of Fluid Mechanics, 2001, vol.426, pp. 177–197.

[10] Graur I.A., Elizarova T.G., Lengrand J.-C.: Numerical computation of shock wave configurations in underexpanded jets. Lab. d'Aérothermique du CNRS, R 99-2, 1999.

[11] Graur I.A., Elizarova T.G, Lengrand J.-C.: Calcul de jets sous-detendus par une approche continue. Lab. d'Aérothermique du CNRS, NT 2001-1, 2001.

[12] Chirokov I.A., Elizarova T.G, Lengrand J.-C.: Calcul tridimensionnel de l'interaction de deux jets sous-detendus par une approche continue, Lab. d'Aérothermique du CNRS, NT 2001 - 2, 2001.

[13] Schlichting H.: Boundary layer theory, Pergamon press, London, 1955.